

Electronic Supplementary Material (ESI) for Nanoscale Horizons.
This journal is © The Royal Society of Chemistry 2019

Synthesis and Optoelectronics of Mixed-Dimensional Bi/Te Binary

Heterostructure

Ye Zhang,^a Jia Guo,^a Yiguo Xu,^b Weichun Huang,^c Chao Li,^a Lingfeng Gao,^a Leiming Wu,^a Zhe Shi,^a Chunyang Ma,^a Yanqi Ge,^a Xiuwen Zhang,^{*b} and Han Zhang^{*a}

a: Institute of Microscale Optoelectronics, Collaborative Innovation Centre for Optoelectronic Science & Technology, Key Laboratory of Optoelectronic Devices and Systems of Ministry of Education and Guangdong Province, College of Physics and Optoelectronic Engineering, Shenzhen Key Laboratory of Micro-Nano Photonic Information Technology, Guangdong Laboratory of Artificial Intelligence and Digital Economy (SZ), Shenzhen University, Shenzhen 518060, P.R. China.

E-mail: hzhang@szu.edu.cn

b: College of Physics and Optoelectronic Engineering, Shenzhen University, Shenzhen 518060, China.

E-mail: xiuwenzhang@szu.edu.cn

c: Nantong Key Lab of Intelligent and New Energy Materials, College of Chemistry and Chemical Engineering, Nantong University, Nantong 226019, Jiangsu, P. R. China

Contents:

1. Experimental Section
2. Table

Table S1. The P_{λ} of light with different wavelength applied in this work.

Table S2. The comparison of the Bi/Te-based PDs with the reported PEC-type PDs.

3. Supporting Figures

Figure S1. AFM images of the synthesized Te NSs and the corresponding height profiles.

Figure S2. a: The sum EDS spectrum of area # 1 obtained from **Figure 1i. b:** The corresponding elements content analysis.

Figure S3. The XPS spectra of Bi/Te. **a:** O 1s region for the fresh Bi/Te. **b-d:** O 1s, Te 3d, and Bi 4f regions for Bi/Te in ambient environment after 7 days.

Figure S4. The color coded 2D maps of Te/Bi.

Figure S5. Partial density of states for a Bi/Te structure with 16 Bi atoms and 36 Te atoms. **a:** by PBE. **b:** by HSE06.

Figure S6. Band alignment between 2D Te and Bi layers by HSE06.

Figure S7. The linear sweep voltammetry (LSV) test of Bi/Te under dark and simulated light (SL, 300-800 nm, level IV).

Figure S8. The photo-response behaviors of the Bi/Te binary heterostructures-based PDs in 0.5 M HCl, KCl, and KOH electrolytes with the bias potential of 0.6 V and the photo-response behaviors of pristine Bi QDs, Te NSs, and Bi/Te-based PDs in 0.5 M KOH electrolyte with the bias potential of 0.6V.

Figure S9. The photo-response behaviors of the Bi/Te binary heterostructures-based PDs in 0.1, 0.5, and 1.0 M KOH electrolytes with the bias potential of 0.3 and 0.6 V, respectively.

Figure S10. The response (t_{res}) and recovery (t_{rec}) time of Bi/Te binary heterostructures-based PDs in 0.5 M KOH electrolyte with different bias potential (a: 0 V, b: 0.3V, and c: 0.6 V).

Figure S11. The long-term stability tests of fresh PD and the PD kept over 30 days for operating 20,000 s with the bias potential of 0 V in 0.5 M KOH electrolyte under SL.

Figure S12. The schematic diagram of the laser platform.

Figure S13. Nonlinear absorption and corresponding fitting curve of fabricated SA based on Bi/Te and microfiber.

1. Experimental Section

Materials: Experimental Details. Sodium tellurite (Na_2TeO_3 , 99.9 %, Aladdin), Bismuth nitrate pentahydrate ($\text{Bi}(\text{NO}_3)_3 \cdot 5\text{H}_2\text{O}$, 99.0 %, Aladdin), aqueous ammonia solution ($\text{NH}_3 \cdot \text{H}_2\text{O}$, 10 % - 35 %, w/w, Acros Organics1), Poly(vinyl pyrrolidone) (PVP, K30, Macklin), hydrazine hydrate ($\text{N}_2\text{H}_4 \cdot \text{H}_2\text{O}$ 85 %, w/w%, Macklin), ethanol (99.9 %), ethylene glycol (EG, 99.9 %), acetone (99.9 %), poly(vinylidene fluoride) (PVDF, $M_n = 71,000 \text{ g mol}^{-1}$), and dimethyl formamide (DMF, 99.9 %) were purchased from Sigma-Aldrich, potassium hydroxide (KOH, 99.5 %), hydrogen chloride (HCl , 16 mol L^{-1}), and potassium chloride (KCl, 99.5 %) were purchased from Sinopharm Chemical Reagent Co., Ltd. Deionized water (DI) was used through the whole process.

Synthesis of Te NSs: Te NSs were prepared as follows: 92 mg Na_2TeO_3 and 1 g PVP were dissolved in 32 mL DI water, then 3.33 mL $\text{NH}_3 \cdot \text{H}_2\text{O}$ and 1.66 mL $\text{N}_2\text{H}_4 \cdot \text{H}_2\text{O}$ were added into the mixture and kept stirring for 30 min. The mixture was poured into a 50 mL hydrothermal kettle for reacting 12 h under 180 °C in a drying oven. After the kettle cooled to room temperature the obtained mixture with silver grey color was washed and centrifuged at 8,000 rpm with DI, ethanol, and acetone, respectively. The supernatant was carefully removed and the precipitate was placed in a vacuum oven at 60 °C overnight for the next use.

Synthesis of Bi/Te binary heterostructures: 20 mg Te NSs and 50 mg $\text{Bi}(\text{NO}_3)_3 \cdot 5\text{H}_2\text{O}$ were dissolved in 20 mL EG through sonication for 10 min. Then the mixture as next transferred into a 50 mL hydrothermal kettle for reacting at 180 °C for 4 h in a drying

oven. As the kettle cooled to room temperature, the obtained mixture with black color was washed and centrifuged at 8,000 rpm with DI, ethanol, and acetone, respectively. The supernatant was carefully removed and the precipitate was placed in a vacuum oven at 60 °C overnight for further characterization and use.

Preparation of Bi/Te binary heterostructures-based working electrode: Typically, 3 mg Bi/Te was added in 1 mL PVDF/DMF (10 mg/100 mL) solution and kept sonication for 30 min to form a homogenous mixture. Then 300 μ L of the mixture was dropped onto the surface of indium tin oxide (ITO)-coated glass and placed in a vacuum oven at 80 °C overnight to form the working electrode for PEC-type photodetection system.

Characterization: The morphology of Bi/Te binary heterostructures was studied by using a GeminiSEM 300 and a FEI Talos 200F TEM (200KV). The optical absorption was measured by an UV-3150 UV-vis-NIR spectrophotometer (Hitachi S4000). The structure and composition of Bi/Te were carried out by using X-Ray Diffraction spectrometer (Rigaku Model D/MAX-2500V/PC) and the Raman spectroscopy (HORIBA Lab RAM HR800) with the excited laser of 633 nm. XPS was applied to examine the Bi/Te with Mg K α radiation as exciting source (ThermoFisher, escalab EI).

Transient absorption spectroscopy: A nondegenerate TA setup is carried out to study the carrier dynamics of Bi/Te. The setup is based on a Ti: sapphire amplifier (Spitfire Ace, Spectra Physics) with ultrafast pulses (800 nm, 1 kHz, 100 fs). The experiment is separated by the splitter into two parts, one is applied to drive the optical parametric

amplifier, which can obtain colinear signal pulses ranging from 1100 to 1600 nm, and the other is the idler pulses ranging from 1600 to 2600 nm. The diameter of pump and probe pulses used in this work are 340 μm and 120 μm , respectively. TA signals are obtained by calculating the absorption difference of Bi/Te under the probe light according to the equation below:

$$\Delta A = A_{0I} - A_{00}$$

where A_{00} is the absorptance without the pump, and A_{0I} is the delay time related absorptance with pump.

Computational Methods: In the present study, the density functional theory (DFT) calculations were performed with Vienna *ab initio* simulation package (VASP) code ^{1, 2}. The projector augmented wave (PAW) potential method was used to describe electron-core interactions. The cut-off energy was selected as 450 eV to expand the electronic wavefunctions under the generalized gradient approximation (GGA) with the Perdew-Burke-Ernzerhof (PBE) exchange-correlation function ³. A vacuum space of at least 20 Å was included in the unit cell to avoid mirror interactions for each case. The theoretical model of Bi/Te was depicted in **Figure 3a**. It contains 62 Bi atoms and 144 Te atoms. Only the Γ point was used for sampling the Brillium zone. The energy minimization was converged when atomic forces are less than 0.01 eV/Å. Van der Waals corrections of optB88-vdW functional was applied for dispersion correction in all calculations ^{4, 5}. Due to the underestimation of energy band gaps through GGA-PBE, the HSE06 hybrid functional is also adopted to correct the band gap values ^{6, 7}.

The photo-response behavior of Bi/Te-based photodetector: The photo-response behaviors were recorded by a PEC-type photodetection system with standard three electrodes as our reported work. The KOH, KCL, and HCl with different concentrations were selected as the electrolytes. Different wavelengths (350 nm, 365 nm, 380nm, 400 nm, 475 nm, 550 nm, and 650 nm) were illuminated on the working electrodes, and the corresponding light power intensities were listed in **Table S1** and used as level I, II, III, IV, and V. For better comparison, the Bi QDs and Te NTs-coated ITO were used as the references and irradiated by the simulated light (SL, 300-800 nm). Linear sweep voltammetry (LSV) was performed from 0 to 1.0 V with a scanning speed of 0.01 V s⁻¹. Amperometric current-time (*I-t*) tests were carried out from 0 to 0.6 V. Electrochemical impedance spectra (EIS) were performed from 1 to 10⁵ Hz with an amplitude of 0.005 V.

Fiber laser experimental setup: In the experiment of mode-locked pulse generation, the schematic of the ring-cavity EDF laser incorporating Bi/Te SAs is shown in **Figure S8**, which including pump source (980 nm), gain fiber (EDF), wavelength division multiplexer (WDM), output coupler (OC), polarization independent isolator (ISO), polarization controller (PC) and Bi/Te SA. Pumped light was transmitted to the ring cavity through a fused WDM. The group velocity dispersion values and length of EDF was -48 ps nm⁻¹ km⁻¹ and 0.8 m, respectively. ISO and PC were used to guarantee the unidirectional operation of the ring cavity and fine tune the polarization state of propagation light, respectively. The mode-locked pulses of the EDF ring resonators were output by using 90/10 OC. The pulse characteristics of these two

lasers were monitored by an optical spectrum analyzer (Yokogawa AQ6370D) and a 1-GHz oscilloscope (Tektronix, MDO4104C) combined with a 5-GHz photodetector (Thorlabs DET08CFC/M). Moreover, by using an optical autocorrelator (APE150 pulsecheck) and a spectrum analyzer (Agilent, N9030A), the pulse width and repetition frequency of mode-locked pulse can be measured.

References:

1. G. Kresse and J. Hafner, *Phys. Rev. B*, 1993, **47**, 558-561.
2. G. Kresse and J. Furthmüller, *Phys. Rev. B*, 1996, **54**, 11169-11186.
3. P. E. Blöchl, *Phys. Rev. B*, 1994, **50**, 17953-17979.
4. J. Klimeš, D. R. Bowler and A. Michaelides, *Phys. Rev. B*, 2011, **83**, 195131.
5. J. Klimeš, D. R. Bowler and A. Michaelides, *J. Phys.: Cond. Matt.*, 2009, **22**, 022201.
6. J. Paier, M. Marsman, K. Hummer, G. Kresse, I. C. Gerber and J. G. Ángyán, *The Journal of chemical physics*, 2006, **124**, 154709.
7. A. V. Krukau, O. A. Vydrov, A. F. Izmaylov and G. E. Scuseria, *J. Chem. Phys.*, 2006, **125**, 224106.

Table S1. The P_λ of light with different wavelength applied in this work.

P_λ (mW/cm ²)	I level	II level	III level	IV level	V level
Simulated light (SL)	26.2	53.0	83.1	118	122
350 nm	0.51	1.02	1.66	2.17	2.19
365 nm	0.764	1.66	2.55	3.57	3.69
380 nm	0.322	1.021	1.908	2.676	2.773
400 nm	0.637	2.04	3.57	5.22	5.35
475 nm	1.91	4.33	7.01	10.1	10.6
550 nm	2.04	3.95	5.98	8.28	8.40
650 nm	2.04	4.08	6.02	8.54	8.92

Table S2. The comparison of the Bi/Te-based PDs with the reported PEC-type PDs.

Materials	Experimental conditions	Responsivity ($\mu\text{A W}^{-1}$)	Detectivity (D^* , Jones)	Ref
Bi/Te NSs	0.5 M KOH, 0.6 V	150.75	5.19×10^9	This work
BP NSs	0.1 M KOH, 0.6 V	5.44	-	8
BP QDs	0.15 M KOH, 0.6V	4.59	7.45×10^8	9
Te NSs	0.1 M KOH, 0.6 V	1.16	2.4×10^6	10
Se NSs	0.1 M KOH, 0.6 V	10.45	-	11
Bi QDs	0.1 M KOH, 0.6 V	8.64	-	12
Sb NSs	0.5 M KOH, 0.6 V	1.5	1.4×10^6	13
PbO QDs	0.01 M KOH, 0.6 V	4280 (400 nm)	-	14
InSe NSs	0.2 M KOH, 1.0V	3.3	-	15
SnS NSs	0.1 M Na_2SO_4 , 0.6 V	17.8	1.92×10^8	16
GeSe NSs	0.1 M KOH, 0.3 V	43.6	6.28×10^{10}	17
Bi_2S_3 NSs	0.1 M KOH, 0.6 V	52	3.75×10^8	18
Te@Se NTs	1.0 M NaOH, 0.6 V	98.31	-	19

Reference:

8. X. Ren, Z. Li, Z. Huang, D. Sang, H. Qiao, X. Qi, J. Li, J. Zhong and H. Zhang, *Adv. Funct. Mater.*, 2017, **27**, 1606834.
9. Y. Zhang, F. Zhang, Y. Xu, W. Huang, L. Wu, Y. Zhang, X. Zhang and H. Zhang, *Adv. Funct. Mater.*, 2019, **29**, 1906610.
10. Z. Xie, C. Xing, W. Huang, T. Fan, Z. Li, J. Zhao, Y. Xiang, Z. Guo, J. Li, Z. Yang, B. Dong, J. Qu, D. Fan and H. Zhang, *Adv. Funct. Mater.*, 2018, **28**, 1705833.
11. T. Fan, Z. Xie, W. Huang, Z. Li and H. Zhang, *Nanotechnol.*, 2019, **30**, 114002.
12. C. Xing, W. Huang, Z. Xie, J. Zhao, D. Ma, T. Fan, W. Liang, Y. Ge, B. Dong, J. Li and H. Zhang, *ACS Photonics*, 2018, **5**, 621-629.
13. L. Su, X. Tang, X. Fan, D. Ma, W. Liang, Y. Li and H. Zhang, *Adv. Funct. Mater.*, 2019, **29**, 1905857.
14. W. Huang, X. Jiang, Y. Wang, F. Zhang, Y. Ge, Y. Zhang, L. Wu, D. Ma, Z. Li, R. Wang, Z. N. Huang, X. Dai, Y. Xiang, J. Li and H. Zhang, *Nanoscale*, 2018, **10**, 20540-20547.
15. Z. Li, H. Qiao, Z. Guo, X. Ren, Z. Huang, X. Qi, S. C. Dhanabalan, J. S. Ponraj, D. Zhang, J. Li, J. Zhao, J. Zhong and H. Zhang, *Adv. Funct. Mater.*, 2018, **28**, 1705237.
16. W. Huang, Z. Xie, T. Fan, J. Li, Y. Wang, L. Wu, D. Ma, Z. Li, Y. Ge, Z. N. Huang, X. Dai, Y. Xiang, J. Li, X. Zhu and H. Zhang, *J. Mater. Chem. C*, 2018, **6**, 9582-9593.
17. D. Ma, J. Zhao, R. Wang, C. Xing, Z. Li, W. Huang, X. Jiang, Z. Guo, Z. Luo, Y. Li, J. Li, S. Luo, Y. Zhang and H. Zhang, *ACS Appl. Mater. Interfaces*, 2019, **11**, 4278-4287.
18. W. Huang, C. Xing, Y. Wang, Z. Li, L. Wu, D. Ma, X. Dai, Y. Xiang, J. Li, D. Fan and H. Zhang, *Nanoscale*, 2018, **10**, 2404-2412.
19. W. Huang, Y. Zhang, Q. You, P. Huang, Y. Wang, Z. N. Huang, Y. Ge, L. Wu, Z. Dong, X. Dai, Y. Xiang, J. Li, X. Zhang and H. Zhang, *Small*, 2019, 1900902.

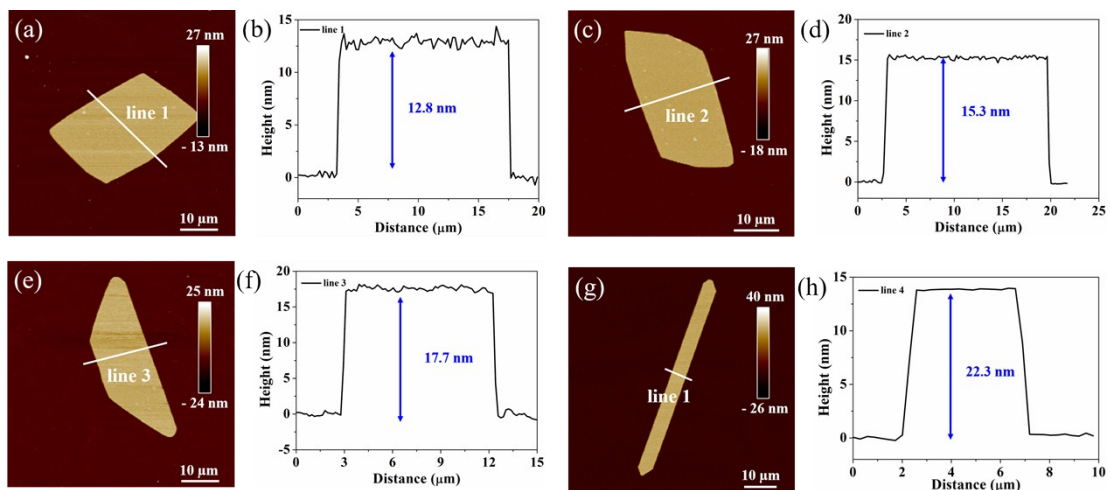
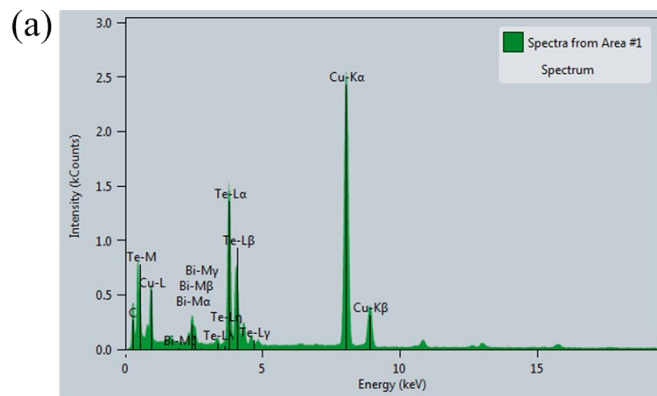


Figure S1. AFM images of the synthesized Te NSs and the corresponding height profiles.



(b)

Z	Element	Family	Atomic Fraction (%)	Atomic Error (%)	Mass Fraction (%)	Mass Error (%)	Fit error (%)
6	C	K	9.27	1.21	1.42	0.11	2.00
29	Cu	K	45.40	8.42	32.51	4.96	0.08
52	Te	L	41.90	6.94	58.22	7.44	0.14
83	Bi	L	3.43	0.56	7.85	0.99	0.40

Figure S2. a: The sum EDS spectrum of area # 1 obtained from **Figure 1i. b:** The corresponding elements content analysis.

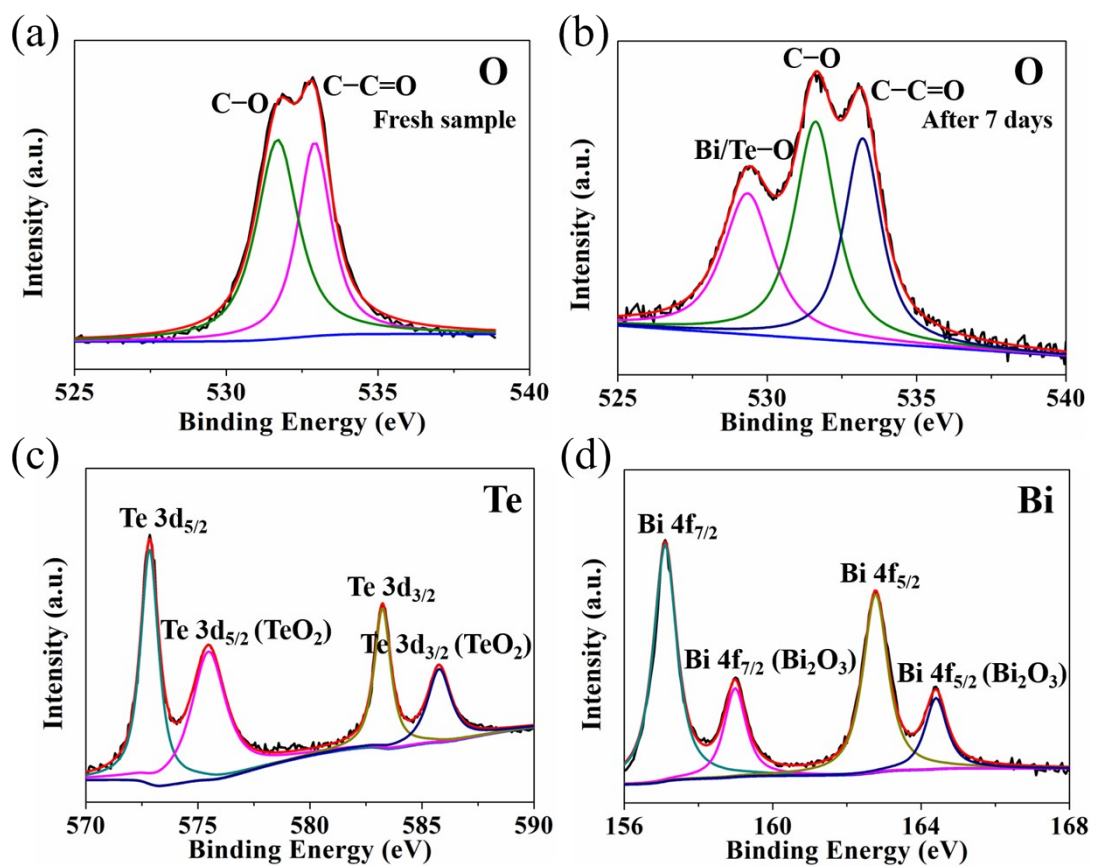


Figure S3. The XPS spectra of Bi/Te. **a:** O 1s region for the fresh Bi/Te. **b-d:** O 1s, Te 3d, and Bi 4f regions for Bi/Te in ambient environment after 7 days.

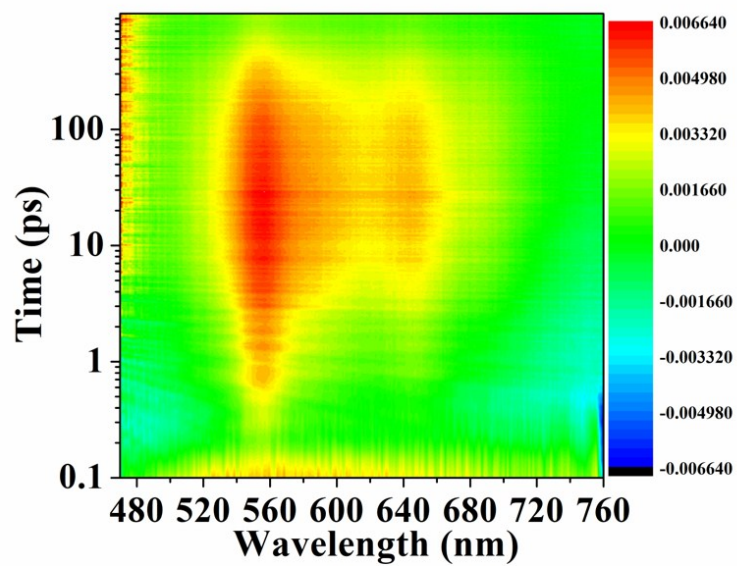


Figure S4. The color coded 2D maps of Bi/Te.

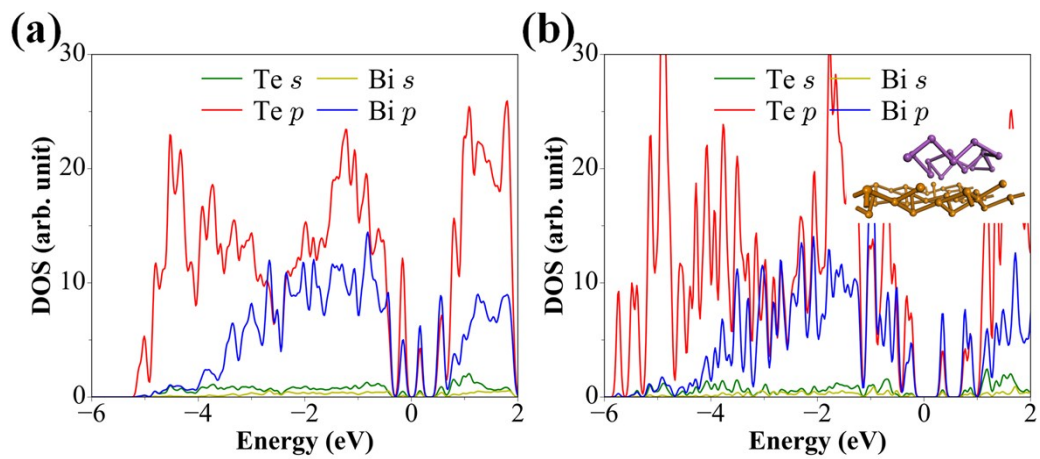


Figure S5. Partial density of states for a Bi/Te structure with 16 Bi atoms and 36 Te atoms. **a:** by PBE. **b:** by HSE06.

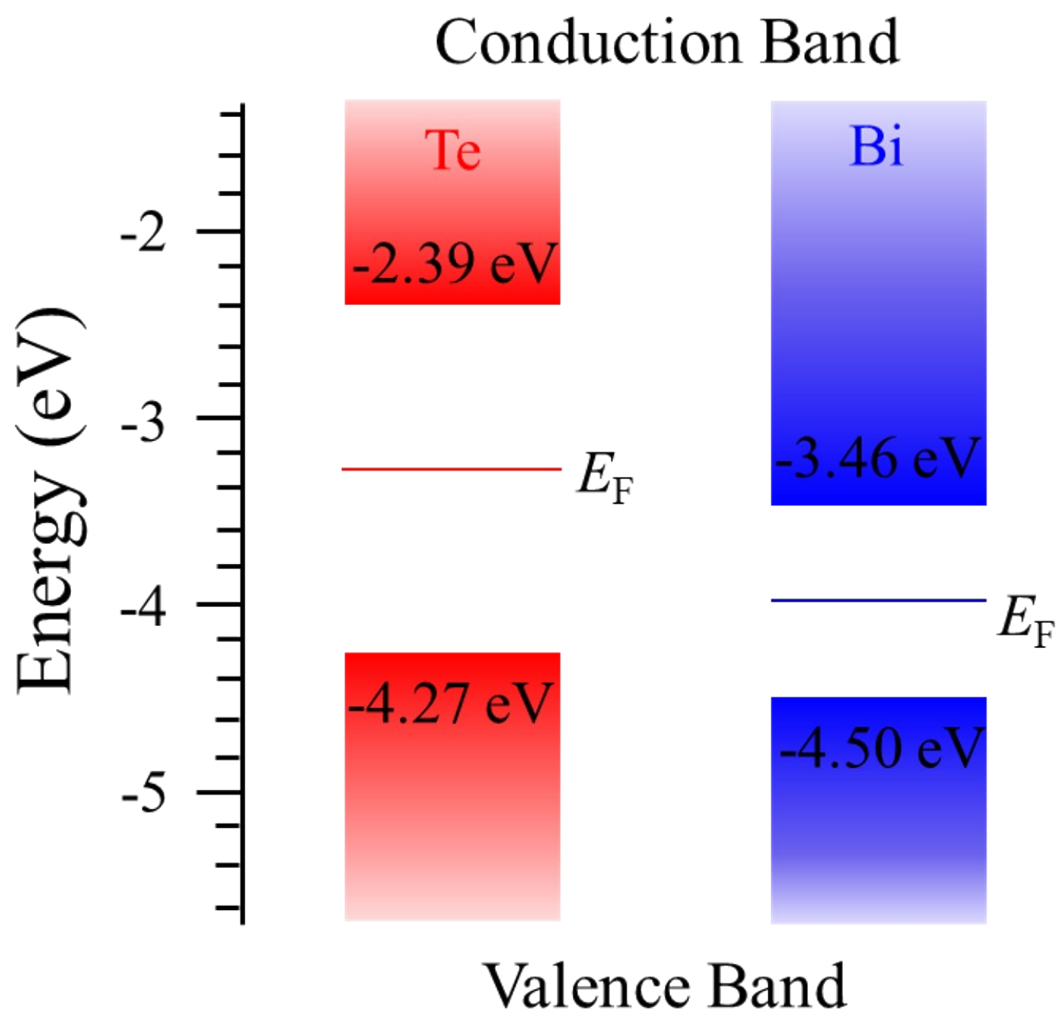


Figure S6. Band alignment between 2D Te and Bi by HSE06.

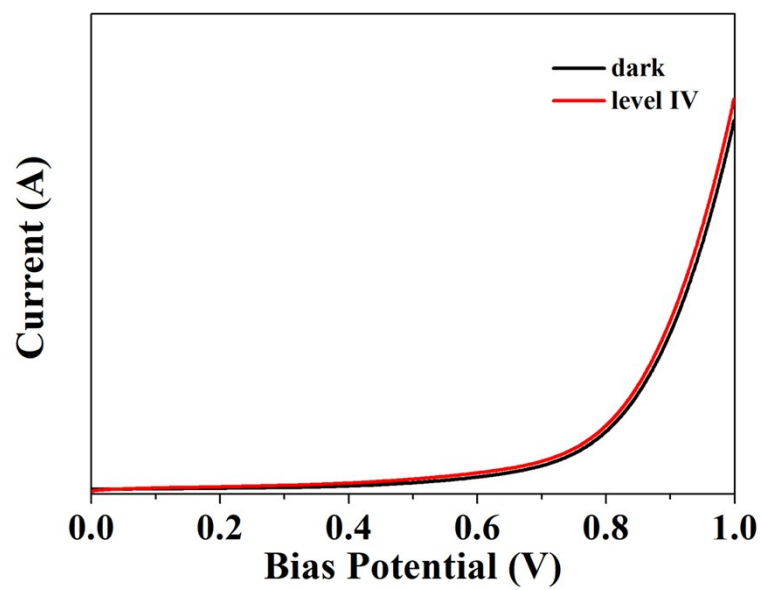


Figure S7. The linear sweep voltammetry (LSV) test of Bi/Te under dark and simulated light (SL, 300-800 nm, level IV).

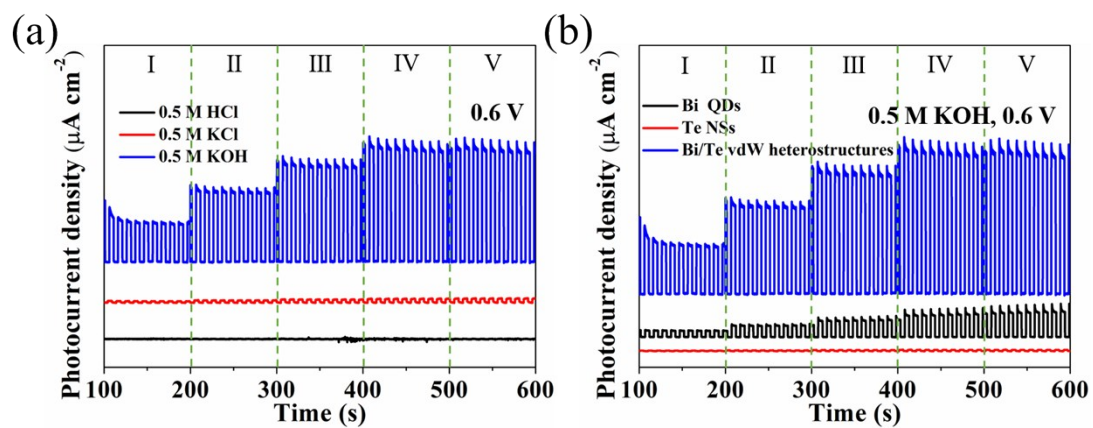


Figure S8. a: The photo-response behaviors of the Bi/Te binary heterostructures-based PDs in 0.5 M HCl, KCl, and KOH electrolytes with the bias potential of 0.6 V. **b:** The photo-response behaviors of pristine Bi QDs, Te NSs, and Bi/Te-based PDs in 0.5 M KOH electrolyte with the bias potential of 0.6V.

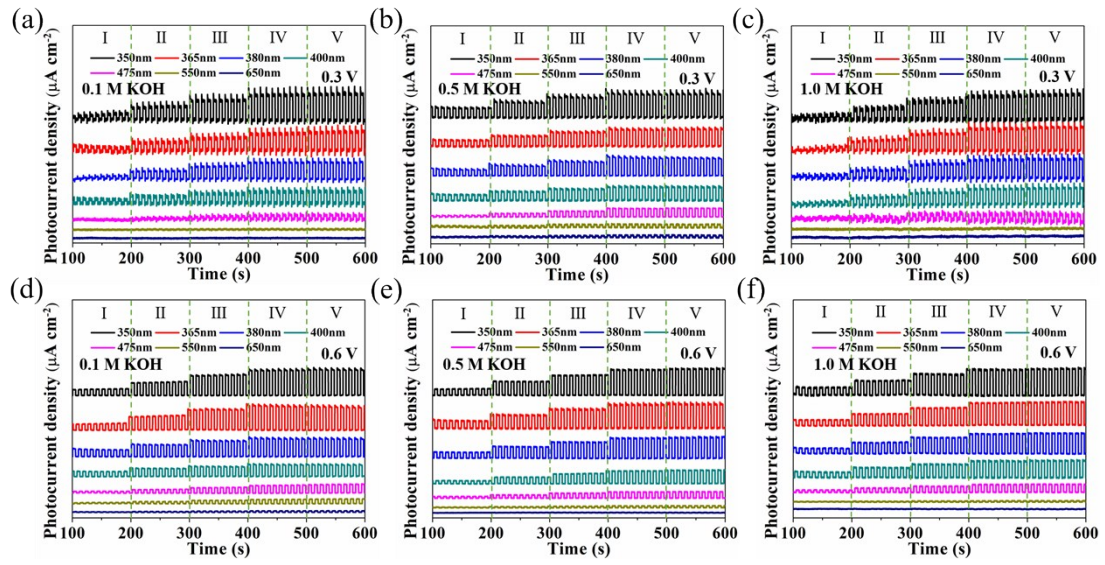


Figure S9. The photo-response behaviors of the Bi/Te binary heterostructures-based PDs in 0.1, 0.5, and 1.0 M KOH electrolytes with the bias potential of 0.3 and 0.6 V, respectively.

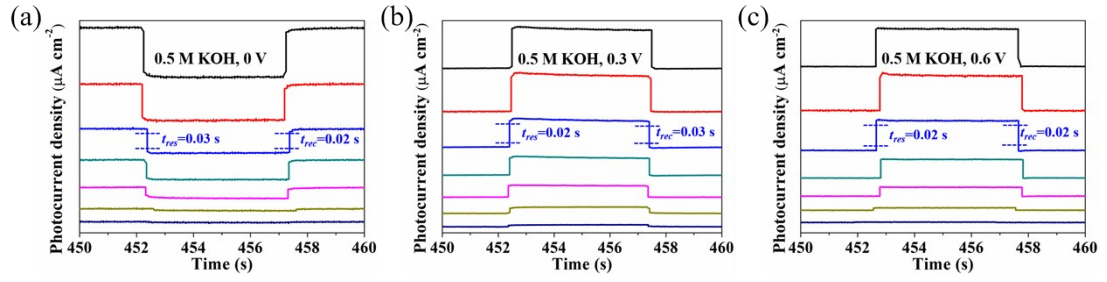


Figure S10. The response (t_{res}) and recovery (t_{rec}) time of Bi/Te binary heterostructures-based PDs in 0.5 M KOH electrolyte with different bias potential (a: 0 V, b: 0.3V, and c: 0.6 V).

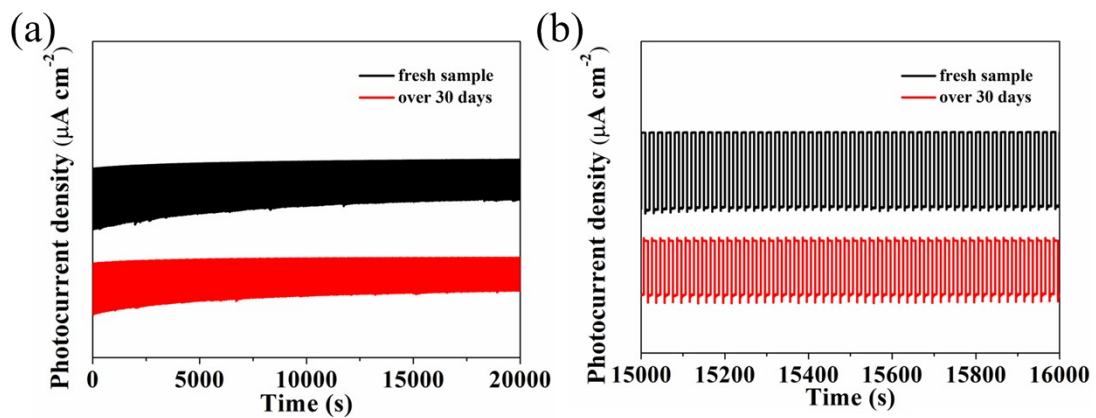


Figure S11. a: The long-term stability tests of fresh PD and the PD kept over 30 days for operating 20,000 s with the bias potential of 0 V in 0.5 M KOH electrolyte under SL. **b:** The selected area of ON/OFF signals from 15,000 to 16,000 s.

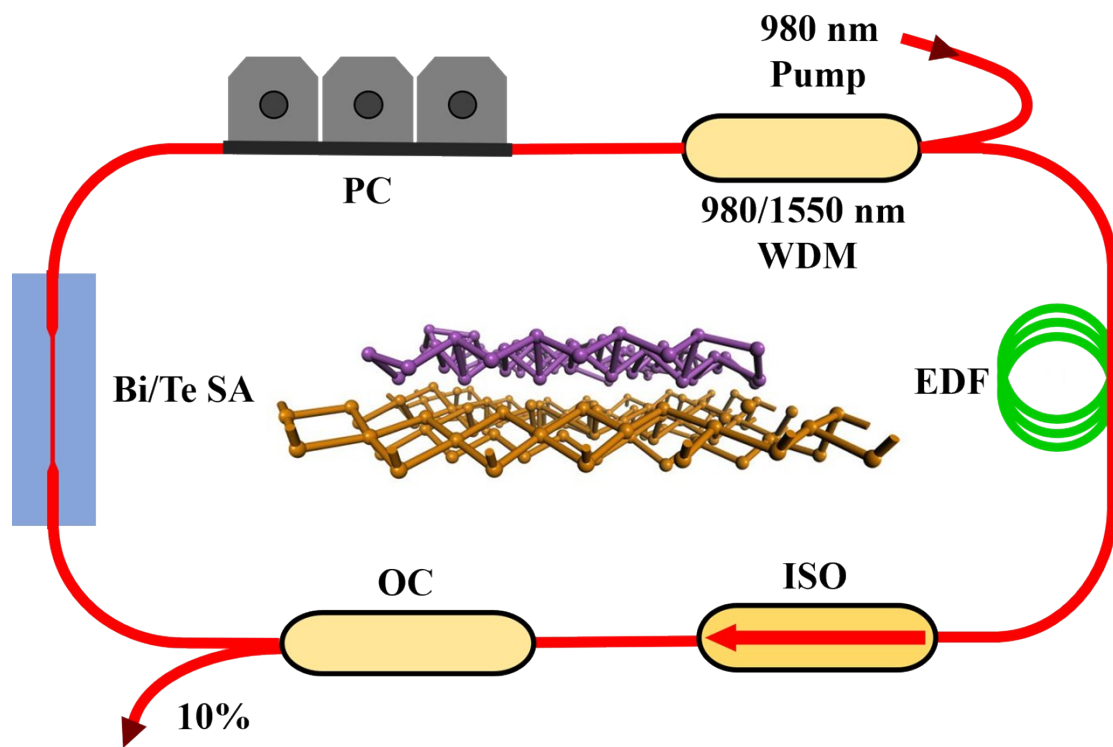


Figure S12. The schematic diagram of the laser platform.

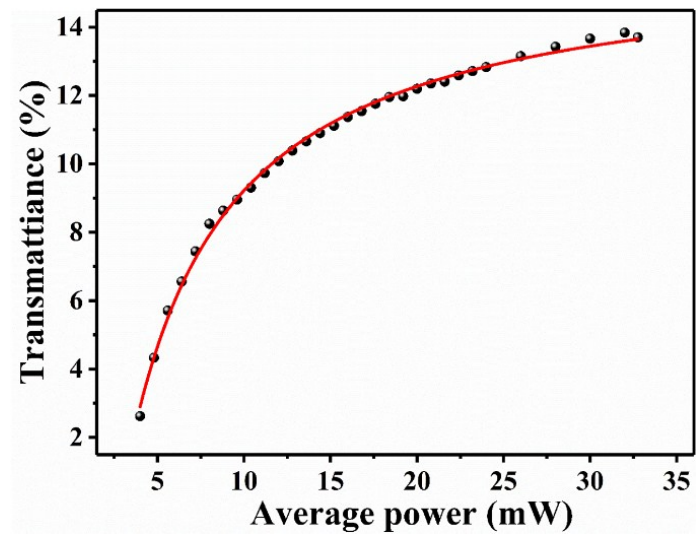


Figure S13. Nonlinear absorption and corresponding fitting curve of fabricated SA based on Bi/Te and microfiber.